

# Synthesis of Light-Controlled Superparamagnetic Core–Shell Structured Nanocomposite for Drug Delivery

Tieyu Chen<sup>1,2,\*</sup>, Tianming Huang<sup>1,†</sup>, and Henry Dai<sup>2</sup>

<sup>1</sup>Guangxi Medical University, Nanning 530021, Guangxi, China

<sup>2</sup>Department of Chemistry, University of Calgary, Calgary, Alberta, T2N 1N4, Canada

This paper reported a core–shell structured site-specific light-controlled magnetic nanocomposite for drug delivery. Its core was composed of superparamagnetic Fe<sub>3</sub>O<sub>4</sub> nanoparticles for magnetic guiding purposes. Its outer shell consisted of mesoporous silica molecular sieve MCM-41 which offered highly ordered hexagonal tunnels for drug molecules. A ligand N1-(5H-cyclopenta [1,2-b:5,4-b'] dipyridin-5-ylidene) benzene-1,4-diamine (denoted as Dafo-Ph-NH<sub>2</sub>) was coupled to the MCM-41 shell. The Dafo end can flip over under 510 nm light therefore will act as a light stimulated acceptor. The final composite was analyzed by electron microscope images, XRD, IR spectra, thermogravimetry, MTT and N<sub>2</sub> adsorption/desorption. Our Dafo-MCM-41@Fe<sub>3</sub>O<sub>4</sub> composite shows light controlled release property for vitamin B<sub>12</sub> *in vitro*.

**Keywords:** Fe<sub>3</sub>O<sub>4</sub> Core, Drug Delivery, Biocompatibility, B<sub>12</sub> Adsorption, Site-Specific, Nanocomposite.

Delivered by Ingenta to: Rice University  
IP: 37.9.40.36 On: Thu, 30 Mar 2017 12:27:04  
Copyright: American Scientific Publishers

## 1. INTRODUCTION

Vitamin B<sub>12</sub> plays a significant role in hematopoiesis, DNA synthesis, cell metabolism and maintains the function of nerve system. To the human, vitamin B<sub>12</sub> can be mainly obtained from the animal derived foods, and its digestive absorption needs the help of gastric acid and intrinsic factor. Vegetarian, atrophic gastritis patients lacking of gastric acid and gastrointestinal diseases patients lacking of intrinsic factor are prone to vitamin B<sub>12</sub> deficiency, and this should lead to further diseases such as pernicious anemia, methylmalonic academia, deprementia, subacute combined degeneration, hyperhomocystinemia, vascular dementia and Alzheimer disease.<sup>1,2</sup> Oral administration is the simplest method to treat the vitamin B<sub>12</sub> deficiency. However the absorption process is slow and quite inefficient. Therefore, developing a new controlled release material is a hot-spot in the application research on Vitamin B<sub>12</sub>.

An ideal drug carrier should have enough capacity of holding drug molecules and the ability to release them at specific tissues, organs on specific time or concentration. Before getting to the morbid tissues, drug carrier should

release as less as possible to avoid the side effects. For the past few years, mesoporous and nanoporous silica based systems for drug delivery, controlled release, and bioseparation have attracted numerous interests. The plenty silanol groups on the surface for modification, which provides a strong frame work for deposition and incorporation of guest molecules to give multifunctional capabilities. Therefore various candidates have been synthesized to be a controlled drug delivery system due to their highly specific surface area, well-ordered pores and large pore volumes.<sup>3–8</sup> A few researchers realized their drawback of the traditional modified mesoporous silicon drug carriers, it is nearly impossible to request a site-specific release from them. Thus, it is needed to explore and develop smart delivery systems with both controllable release and site-specific character, and proposed Core–shell structured nanocomposites to meet the above requirements.<sup>9,10</sup> However, the modification on controllable and active release is rarely seen. Thus, in this effort, we try to construct a composite with the two properties: site-specific delivery, and light controlled smart release. To obtain the above properties, we synthesized a composite where Fe<sub>3</sub>O<sub>4</sub> and MCM-41 are applied as inner core and outer shell, respectively. An organic ligand was grafted into MCM-41 tunnels aiming at releasing drug under light stimulating. This magnetic

\*Author to whom correspondence should be addressed.

†These two authors contributed equally to this work.

nanocomposite is further considered and evaluated for site-specific and controlled release drug delivery.

## 2. EXPERIMENTAL DETAILS

### 2.1. Reagents and Instruments Information

Starting chemicals of this work are listed below. 1,10-phenanthroline, benzene-1,4-diamine, KOH,  $\text{KMnO}_4$ , tetraethoxysilane (TEOS, AR), odium dodecyl sulfate (SDS, AR), cetyltrimethylammonium bromide (CTAB, AR),  $\text{FeCl}_3$  (AR), *p*-toluene sulfonic acid, (3-Bromopropyl)trimethoxysilane (BPTS, AR),  $\text{NH}_3 \cdot \text{H}_2\text{O}$  (28 wt%), vitamin  $\text{B}_{12}$  and concentrated HCl were all bought from Sigma-Aldrich. Organic solvents used in this work, such as anhydrous ethanol, toluene, glycol,  $\text{CHCl}_3$ , *n*-hexane (AR) and tetrahydrofuran (THF), were purchased from Sigma-Aldrich. Solvent water was deionized.

Equipment information is summarized as follows. A Perkin-Elmer Spectrum 100 FTIR spectrometer ( $400\text{--}4000\text{ cm}^{-1}$ , KBr pellet technique), a Bruker AVANCE 300 spectrometer, and an Agilent 1100 MS series/AXIMA CFR MALDI/TOF MS spectrometer were used to record IR, NMR and MS spectra, respectively. Magnetic property was obtained from a MPM5-XL-5 superconducting quantum interference device. XRD measurement was performed by a Rigaku Multiflex X-ray diffractometer ( $\lambda = 1.5418\text{ \AA}$ ).  $\text{N}_2$  adsorption and desorption measurement was taken with a Nova 1000 analyzer. Pore size and volume were calculated by Barrett-Joyner-Halenda (BJH) model. Sample morphology was recorded with a Hitachi S-4800 microscope and a JEOL JEM-2010 transmission electron microscope, respectively. Sample thermal degradation was analyzed by a Perkin-Elmer STA 6000 thermal analyzer. Vitamin  $\text{B}_{12}$  concentrations were recorded through a LAMBDA 25 UV/Vis spectrophotometer. The OD reading in the cytotoxicity testing was obtained via a Beckman DTX 880 microplate reader at a wavelength of 595 nm. Above operations were carried out in the air at room temperature with no specifications.

### 2.2. Synthesis of Dafo-Ph-NH<sub>2</sub>

N1-(5H-cyclopenta[1,2-b:5,4-b']dipyridin-5-ylidene)benzene-1,4-diamine (denoted as Dafo-Ph-NH<sub>2</sub>) was prepared following a two-step procedure described as follows. Firstly, 5H-cyclopenta[1,2-b:5,4-b']dipyridin-5-one (Dafo) was prepared with 1,10-phenanthroline as starting reagent following a literature procedure.<sup>11</sup> Then, Dafo (10 mmol), benzene-1,4-diamine (12 mmol), *p*-toluene sulfonic acid (1 mmol) and toluene (150 mL) were mixed together and heated to reflux for 8 hours under Ar protection. Crude production was purified by recrystallization from ethanol/toluene to give Dafo-Ph-NH<sub>2</sub> as dark red powder. <sup>1</sup>H NMR ( $\text{CDCl}_3$ ): *d* 8.77 (*s*, 1H), 8.64 (*s*, 1H), 8.25 (*s*, 1H), 7.37 (*s*, 2H), 7.03–6.98 (*m*, 3H), 6.81–6.79 (*m*, 2H), 5.03(*s*, 2H). MS *m/z*: [*m*+1]<sup>+</sup> calc. for  $\text{C}_{17}\text{H}_{12}\text{N}_4$ , 272.1; found, 273.1.

### 2.3. Construction of BPTS-MCM-41@Fe<sub>3</sub>O<sub>4</sub>

The core-shell supporting matrix BPTS-MCM-41@Fe<sub>3</sub>O<sub>4</sub> was prepared in a four-step procedure as following. First, the magnetic nanoparticles Fe<sub>3</sub>O<sub>4</sub> core was synthesized with  $\text{FeCl}_3 \cdot 6\text{H}_2\text{O}$  as starting material.<sup>12,13</sup> To 150 mL glycol was added  $\text{FeCl}_3 \cdot 6\text{H}_2\text{O}$  (4 g), SDS (1.5 g) and NaAc (11 g). The mixture was held still at room temperature for 30 min then transferred to a teflon flask. This flask was sealed into an autoclave and heated to 200 °C overnight. After cooled to room temperature, the solid product was filtered and rinsed by distilled water. Then this magnetic nanoparticle core was coated with amorphous silica. To 200 mL ethanol, 1 g Fe<sub>3</sub>O<sub>4</sub> was added, kept stirring under ultrasonics for 20 min, then added another 150 mL ethanol, 75 mL deionized water, 5 mL ammonia and 2 g TEOS. This mixture was further stirred at room temperature for 5 hours then centrifuged. Crude product ( $\text{SiO}_2\text{@Fe}_3\text{O}_4$ ) was collected and washed with distilled water.

Silica molecular sieve MCM-41 was further planted on  $\text{SiO}_2\text{@Fe}_3\text{O}_4$  following below steps. To a solution of 160 mL deionized water, 120 mL ethanol and 5 mL ammonia, was added  $\text{SiO}_2\text{@Fe}_3\text{O}_4$  (1 g), CTAB (0.8 g). The mixture was stirred under ultrasonics for 15 minutes. Then TEOS (2 g) was added at drop-wise into the suspension and allowed to react at room temperature overnight. Quenched the reaction by centrifugation. Then dispersed the solid compound again with 300 mL ethanol and 20 mL HCl. This mixture was stirred at room temperature overnight to remove CTAB. The resulting solid product (MCM-41@Fe<sub>3</sub>O<sub>4</sub>) was collected and washed with plenty of water. The product was dried under vacuum at 60 °C.

MCM-41@Fe<sub>3</sub>O<sub>4</sub> was finally linked with silane coupling reagent BPTS. To a solution of 150 mL dry toluene was added 1 g MCM-41@Fe<sub>3</sub>O<sub>4</sub> and 0.5 g BPTS, then heated the suspension to reflux under Ar protection overnight. The resulting solid sample (BPTS-MCM-41@Fe<sub>3</sub>O<sub>4</sub>) was centrifuged and washed with 200 mL benzene and then 200 mL ethanol. The solid product was dried under vacuum at 60 °C overnight.

### 2.4. Construction of Dafo-MCM-41@Fe<sub>3</sub>O<sub>4</sub>

The drug carrier: site-specific superparamagnetic composite Dafo-MCM-41@Fe<sub>3</sub>O<sub>4</sub> was constructed as following procedures. To a solution of 120 mL dry toluene was added 1.5 g anhydrous potassium carbonate, 0.3 g Dafo-Ph-NH<sub>2</sub> and 0.6 g BPTS-MCM-41@Fe<sub>3</sub>O<sub>4</sub>, then raised the temperature to reflux under stirring for 3 days. After cooled to room temperature, the solid product was centrifuged, collected and washed with distilled water to remove potassium carbonate, then dried in vacuum at 60 °C and obtained as Dafo-functionalized supporting matrix.

### 2.5. In Vitro Cytotoxicity of the Dafo-MCM-41@Fe<sub>3</sub>O<sub>4</sub>

The *in vitro* cytotoxicity of the Dafo-MCM-41@Fe<sub>3</sub>O<sub>4</sub> was determined by MTT assays, and the L929 fibroblast

cell line was used here. L929 fibroblast cell in 200  $\mu\text{L}$  media per well were plated in a 96-well plate for 24 h to allow the cells to attach and then exposed to different concentrations of the Dafo-MCM-41@Fe<sub>3</sub>O<sub>4</sub> (1.5625, 3.125, 6.25, 12.5, 25.0, 50.0  $\mu\text{g mL}^{-1}$ ) for 24 h in 5% CO<sub>2</sub> at 37 °C. After that, the medium containing the Dafo-MCM-41@Fe<sub>3</sub>O<sub>4</sub> was removed and MTT solution (20  $\mu\text{L}$  diluted in a culture medium to a final concentration of 5 mg/mL) was added. Incubated again in the incubator for another 4 h, replace the solvent in the wells by 100  $\mu\text{L}$  DMSO, and the absorbance was monitored with a microplate reader at a wavelength of 595 nm. All tests were performed in triplicate. The cell viability was calculated using the following equation:

$$\text{Cell viability (\%)} = [A]_{\text{test}}/[A]_{\text{control}} \times 100\%$$

### 2.6. Vitamin B<sub>12</sub> Loading and Release *In Vitro*

200 mg of Dafo-MCM-41@Fe<sub>3</sub>O<sub>4</sub> was suspended in 20 mL ethanol solution of vitamin B<sub>12</sub> with a concentration of 40 mg/mL at room temperature under stirring for two overnight under 510 nm radiation to achieve drug loading equilibrium. After Dafo-MCM-41@Fe<sub>3</sub>O<sub>4</sub> was connected with the drug (denoted as B<sub>12</sub>-Dafo-MCM-41@Fe<sub>3</sub>O<sub>4</sub>), the composite was collected by centrifugation, washed gently by ethanol, and dried at 60 °C under vacuum overnight. The amount of vitamin B<sub>12</sub> loaded was determined as 0.12 mmol/g (against unloaded Dafo-MCM-41@Fe<sub>3</sub>O<sub>4</sub> by concentration difference before and after Dafo-MCM-41@Fe<sub>3</sub>O<sub>4</sub> loading with UV-vis absorption spectrophotometry). 100 mg of the obtained dry samples was compressed into disk for drug release. After drug was loaded, the B<sub>12</sub>-loaded Dafo-MCM-41@Fe<sub>3</sub>O<sub>4</sub> drug disks were put into 20 mL simulated body fluid (SBF, pH = 7.4) maintained at 37 °C and stirred gently. At predetermined time intervals, 0.5 mL of the sample was withdrawn and immediately replaced with the same amount of SBF buffer to keep the volume constant. The withdrawn solution fractions were monitored by UV-vis spectrophotometer at a wavelength of 360 nm.

## 3. RESULTS AND DISCUSSION

### 3.1. Design Strategy of Dafo-MCM-41@Fe<sub>3</sub>O<sub>4</sub>

Scheme 1 illustrates the construction procedures of the site specific complex Dafo-MCM-41@Fe<sub>3</sub>O<sub>4</sub> and the drug loading mechanism. A typical core–shell structure is observed for Dafo-MCM-41@Fe<sub>3</sub>O<sub>4</sub>, where Fe<sub>3</sub>O<sub>4</sub> acts as inner core while MCM-41 acts as outer shell. The Fe<sub>3</sub>O<sub>4</sub> core is clearly chosen for purpose of site-specific magnetic guiding. Its outer shell consisted of mesoporous silica molecular sieve MCM-41 which offered highly ordered hexagonal tunnels for drug molecules.<sup>12,13</sup> The thin amorphous SiO<sub>2</sub> crust between Fe<sub>3</sub>O<sub>4</sub> core and MCM-41 shell was built to decrease magnetic aggregation between Fe<sub>3</sub>O<sub>4</sub> particles and thus facilitates MCM-41 growth. The end of ligand can flip over under light irradiation in the

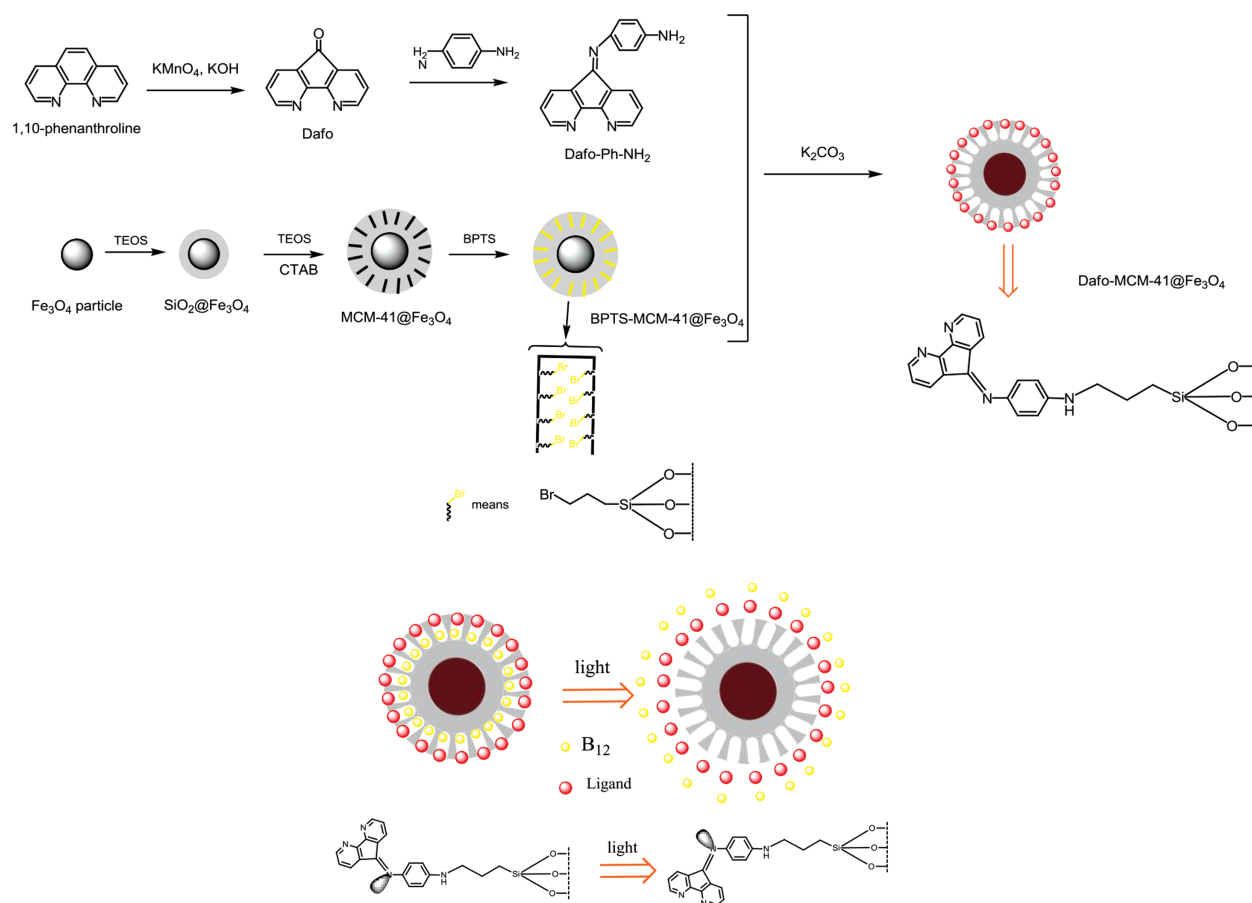
MCM-41 tunnels and change the tunnels' diameter, thus can release drug molecules when the tunnels changing size. It is contemplated this core–shell structured composite is able to release the drug molecules under light stimulated and to achieve a complete and efficient site-specific delivery.

### 3.2. Morphology and Magnetic Feature of Dafo-MCM-41@Fe<sub>3</sub>O<sub>4</sub>

Morphology of our prepared samples were analyzed by their SEM images shown in Figure 1. The Fe<sub>3</sub>O<sub>4</sub> particles have an uneven surface and poor dispersal with mean diameter of about 125 nm. Aggregation can be explained by their magnetic properties. The surface of nanoparticle are full of small hunches and humps. However, after being coated with amorphous SiO<sub>2</sub>, the nanoparticles' surface became smooth, and the diameter increased to about 155 nm. On the other hand, a better dispersion can be seen on SiO<sub>2</sub>@Fe<sub>3</sub>O<sub>4</sub> which means that the SiO<sub>2</sub> layer can significantly reduce the attraction between those magnetic particles. With this improved sample surface as well as dispersal, MCM-41 growth on SiO<sub>2</sub>@Fe<sub>3</sub>O<sub>4</sub> has been readily performed. As what we expected, MCM-41 growth on the SiO<sub>2</sub>@Fe<sub>3</sub>O<sub>4</sub> increased the diameter to about 280 nm, with nearly mono-dispersal, as shown in Figure 1. After BPTS coupling, the mean diameter of BPTS-MCM-41@Fe<sub>3</sub>O<sub>4</sub> shows no increase, suggesting that BPTS is connected into MCM-41 tunnels rather than sample surface. After Dafo-Ph-NH<sub>2</sub> connected, morphology and diameter of Dafo-MCM-41@Fe<sub>3</sub>O<sub>4</sub> are close to BPTS-MCM-41@Fe<sub>3</sub>O<sub>4</sub>. This core–shell structure is further confirmed by transmission electron microscope (TEM) of Dafo-MCM-41@Fe<sub>3</sub>O<sub>4</sub> shown in Figure 1. Upon the above facts, it can be concluded that the Dafo-MCM-41@Fe<sub>3</sub>O<sub>4</sub> has been constructed, with its core width of 125 nm and MCM-41 shell width of 70 nm.

In this research, the Fe<sub>3</sub>O<sub>4</sub> core is designed for site-specific drug delivery purpose, therefore it should be magnetic guiding. The Magnetic feature of Fe<sub>3</sub>O<sub>4</sub>, SiO<sub>2</sub>@Fe<sub>3</sub>O<sub>4</sub> and Dafo-MCM-41@Fe<sub>3</sub>O<sub>4</sub> can be seen in Figure 2. All those particles show superparamagnetic behavior there is no hysteresis. The saturation magnetization value of Fe<sub>3</sub>O<sub>4</sub> is 82 emu/g. According to the literature, iron oxide particles larger than 30 nm should not have superparamagnetic behavior.<sup>14</sup> It was, however, not work in our case. In Fe<sub>3</sub>O<sub>4</sub> tiny bumps and humps bearing the surface, we assume that all of these Fe<sub>3</sub>O<sub>4</sub> particles are actually made up of tiny subatomic smaller than 30 nm. After coated by SiO<sub>2</sub>, the saturation values declined to 75 emu/g. The magnetization values declined to 35 emu/g after the particle was further coated with MCM-41 and ligand. These decreased values compared to saturation value of Fe<sub>3</sub>O<sub>4</sub> nanoparticles can be explained by their decreased Fe<sub>3</sub>O<sub>4</sub> weight ratios.

Owing to its hydrophilic surface and supermagnetic nature, Dafo-MCM-41@Fe<sub>3</sub>O<sub>4</sub> can be easily dispersed in



**Scheme 1.** Synthetic procedure and the drug releasing mechanism on the site-specific composite Dafo-MCM-41@Fe<sub>3</sub>O<sub>4</sub>.

water, forming a stable suspension. And in the magnet field, can be readily aggregated to a specific site which verified our purpose of designing on this compound: site-specific guiding. The above properties can be seen in the Figure 3.

### 3.3. *In Vitro* Cytotoxicity of the Dafo-MCM-41@Fe<sub>3</sub>O<sub>4</sub> Composites

Since our Dafo-MCM-41@Fe<sub>3</sub>O<sub>4</sub> nanoparticle was designed to act as a drug carrier, the biocompatibility of the composites must be studied. Therefore an MTT assay was performed on these Dafo-MCM-41@Fe<sub>3</sub>O<sub>4</sub> nanoparticle. This method is based on the formation of dark red formazan by the live cells after their exposure to MTT (3-(4,5-dimethylthiazol-2-yl)-2,5-diphenyltetrazolium bromide). Cell viability is directly proportional to the amount of formazan produced monitored by the absorbance at 595 nm. The concentration of our tested particle was prepared from (1.5625–50 μg/mL). Figure 4 shows the cell viability of L929 fibroblast cell incubated with the composites. As shown on Figure 4, no significant cytotoxicity is observed in the Dafo-MCM-41@Fe<sub>3</sub>O<sub>4</sub> composite in our experiment. And we prudentially believe it is biocompatible for drug delivery.

### 3.4. XRD Analysis

To understand the internal structure of our nanoparticles, XRD analysis was carried forward on Dafo-MCM-41@Fe<sub>3</sub>O<sub>4</sub> and Fe<sub>3</sub>O<sub>4</sub> particles. Figure 5 shows the wide angle XRD (WAXRD) patterns of the above composites. WAXRD pattern of Dafo-MCM-41@Fe<sub>3</sub>O<sub>4</sub> particle is close to Fe<sub>3</sub>O<sub>4</sub> particles, which means that the magnetic core in Dafo-MCM-41@Fe<sub>3</sub>O<sub>4</sub> has been well preserved after silica coating and drug loading procedures. There are six detectable diffraction peaks in each curve, marked as (220), (311), (400), (422), (551), (440), which is consistent with literature reports.<sup>9,10,12,13</sup> Their different diffraction intensity values can be explained by the silica shell on Dafo-MCM-41@Fe<sub>3</sub>O<sub>4</sub> surface which weakens sample regularity. Small-angle XRD (SAXRD) patterns of Dafo-MCM-41@Fe<sub>3</sub>O<sub>4</sub>, and MCM-41@Fe<sub>3</sub>O<sub>4</sub> are shown in Figure 6. A strong Bragg reflection peak indexed as (200) and two weak peaks indexed as (1 0 0) and (1 1 0) can be observed from both samples, suggesting that there are mesostructure on their surface.<sup>9,10</sup> The intensity difference between two curves can be explained by the ligand modification and drug loaded on it which partially compromised these highly ordered structure. We hereby tentatively confirmed that MCM-41 molecular

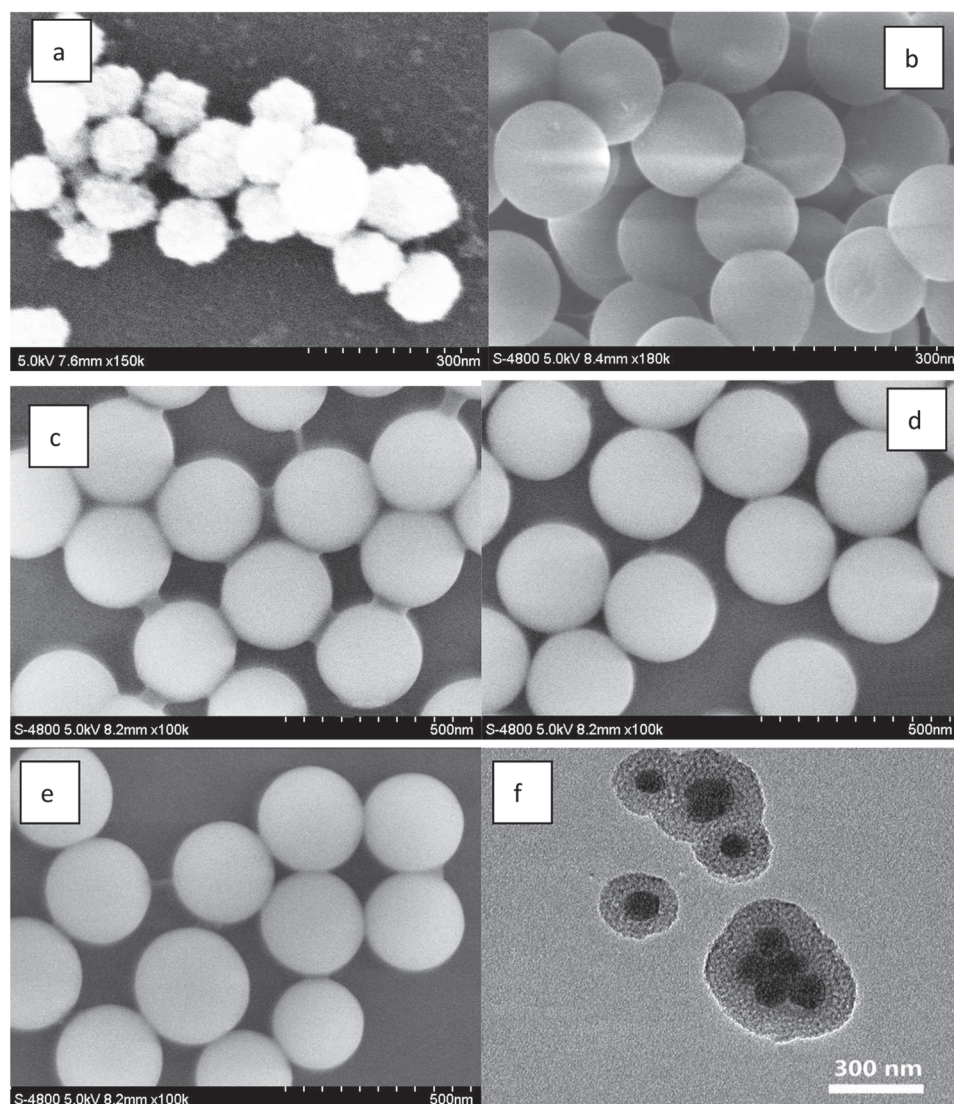


**Figure 1.** SEM images of  $\text{Fe}_3\text{O}_4$  particles (a),  $\text{SiO}_2@ \text{Fe}_3\text{O}_4$  (b),  $\text{MCM-41}@ \text{Fe}_3\text{O}_4$  (c),  $\text{BPTS-MCM-41}@ \text{Fe}_3\text{O}_4$  (d)  $\text{Dafo-MCM-41}@ \text{Fe}_3\text{O}_4$  (e), along with the TEM of  $\text{Dafo-MCM-41}@ \text{Fe}_3\text{O}_4$  (f).

sieve has been constructed as the outer shell of  $\text{Fe}_3\text{O}_4$  core.

### 3.5. $\text{N}_2$ Adsorption/Desorption

As we mentioned above, our purpose of synthesizing this composite is to meet the requirement of holding the drug molecules. Therefore the ligand modified MCM-41 shell was analyzed by  $\text{N}_2$  adsorption/desorption measurement. Figure 7 shows adsorption/desorption isotherms of  $\text{Dafo-MCM-41}@ \text{Fe}_3\text{O}_4$ ,  $\text{MCM-41}@ \text{Fe}_3\text{O}_4$  and  $\text{B}_{12}\text{-Dafo-MCM-41}@ \text{Fe}_3\text{O}_4$ . Despite of their different intensity values, these isotherms are all type-IV ones and similar to each other, suggesting that regular hexagonal tunnels have been successfully constructed on  $\text{Fe}_3\text{O}_4$  core and well preserved after silica coating/probe loading procedures.<sup>15, 16</sup> For  $\text{MCM-41}@ \text{Fe}_3\text{O}_4$ , surface area, pore volume and pore diameter are  $678.2 \text{ m}^2 \cdot \text{g}^{-1}$ ,  $0.462 \text{ cm}^3 \cdot \text{g}^{-1}$  and 2.82 nm,

respectively, which are close to literature values.<sup>17, 18</sup> After ligand growing procedure, above value of  $\text{Dafo-MCM-41}@ \text{Fe}_3\text{O}_4$  decrease to  $468 \text{ m}^2 \cdot \text{g}^{-1}$ ,  $0.31 \text{ cm}^3 \cdot \text{g}^{-1}$  and 2.64 nm. Drug loading procedure further decreases above value of  $\text{B}_{12}\text{-Dafo-MCM-41}@ \text{Fe}_3\text{O}_4$  to  $394 \text{ m}^2 \cdot \text{g}^{-1}$ ,  $0.28 \text{ cm}^3 \cdot \text{g}^{-1}$  and 2.33 nm. All these changes in the parameters confirmed the introduction of the drug molecules into the pores of the composites.

### 3.6. Determination of Drug Loading

FT-IR spectrum are demonstrated to understand the change of the functionalized process and the interaction between the drug and composites. From Figure 8, all three composites shows strong peaks at around  $3430 \text{ cm}^{-1}$  and  $1080 \text{ cm}^{-1}$ . The vibration of C–O and the association absorption of –OH account for these two peaks.  $\text{MCM-41}@ \text{Fe}_3\text{O}_4$  IR spectrum is a simple one with several

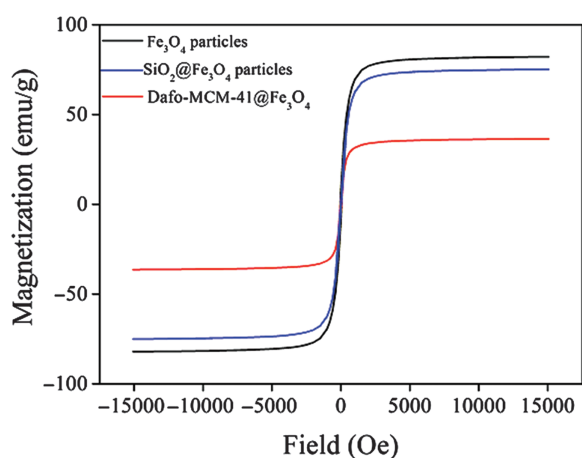


**Figure 2.** Magnetic feature of  $\text{Fe}_3\text{O}_4$  and  $\text{SiO}_2@Fe_3O_4$  particles and  $\text{Dafo-MCM-41}@Fe_3O_4$ .

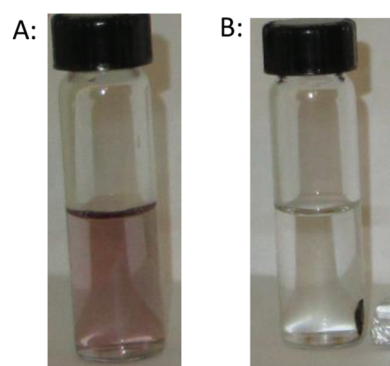


**Figure 3.** Photos of  $\text{Dafo-MCM-41}@Fe_3O_4$  in ethanol solution in the absence of magnetic field and presence of magnetic field.

characteristic bands peaking at  $458\text{ cm}^{-1}$ ,  $604\text{ cm}^{-1}$ ,  $802\text{ cm}^{-1}$  and  $1644\text{ cm}^{-1}$ , respectively. These bands are attributed to plane bending and stretching of Si-O-Si framework, indicating the presence of silica coating shell. These bands are well preserved in  $\text{Dafo-MCM-41}@Fe_3O_4$  and  $\text{B}_{12}\text{-Dafo-MCM-41}@Fe_3O_4$  IR spectrum.

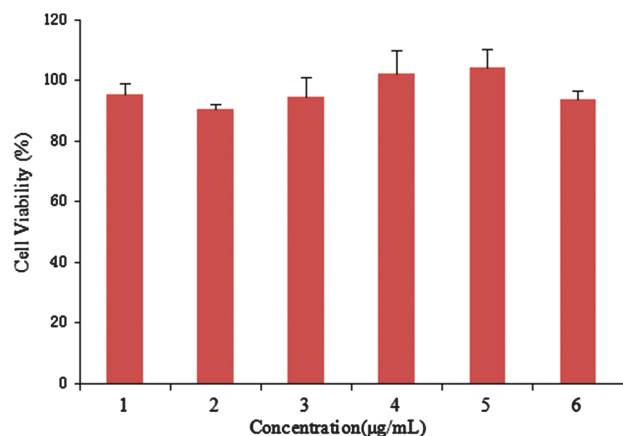


**Figure 4.** Cell viability of L929 fibroblast cells incubated with  $\text{Dafo-MCM-41}@Fe_3O_4$ .

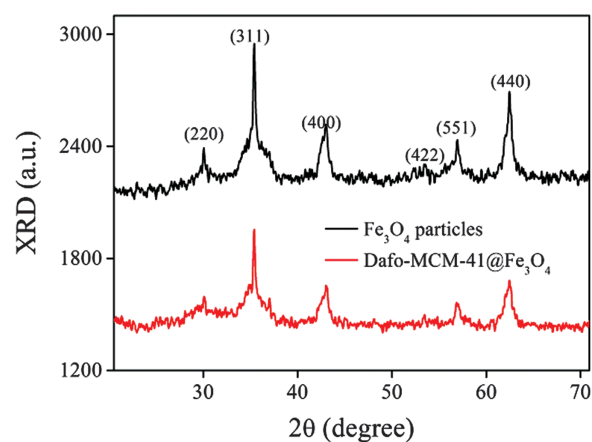


**Figure 5.** WAXRD patterns of  $\text{Dafo-MCM-41}@Fe_3O_4$  and  $\text{Fe}_3\text{O}_4$  particles.

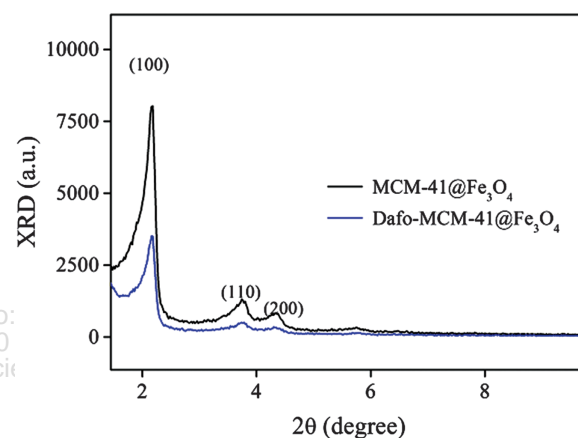


**Figure 6.** SAXRD of  $\text{Dafo-MCM-41}@Fe_3O_4$  and  $\text{MCM-41}@Fe_3O_4$ .

When Dafo is connected to the MCM-41 shell, new peaks of  $2960\text{ cm}^{-1}$ ,  $1680\text{ cm}^{-1}$  and  $1508\text{ cm}^{-1}$  can be seen on the spectrum, which can be assigned to vibration of C=N group and the vibration of -NH group.<sup>11</sup> In the IR of  $\text{B}_{12}\text{-MCM-41}@Fe_3O_4$ , the ratio of

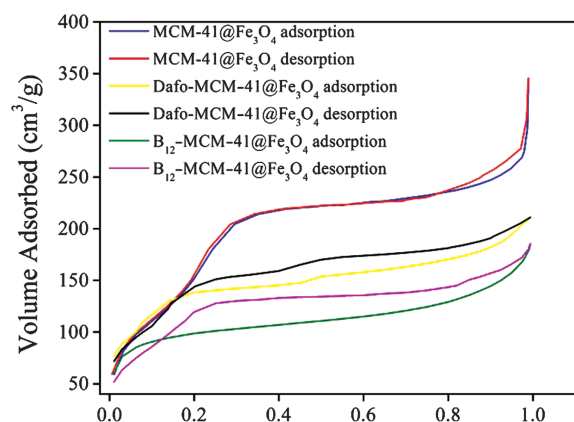


**Figure 7.**  $\text{N}_2$  adsorption/desorption isotherms of  $\text{B}_{12}\text{-Dafo-MCM-41}@Fe_3O_4$ ,  $\text{Dafo-MCM-41}@Fe_3O_4$  and  $\text{MCM-41}@Fe_3O_4$ .

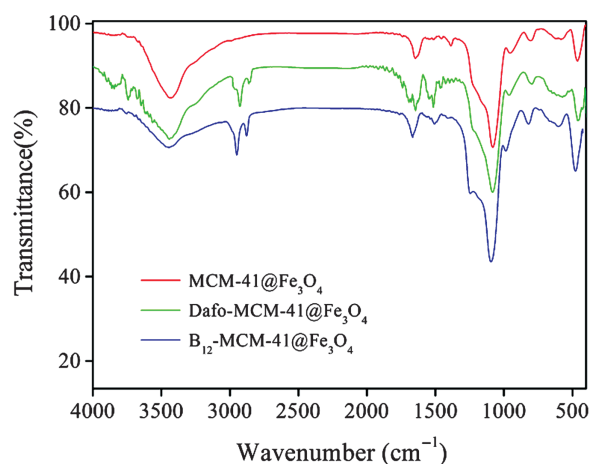


**Figure 8.** IR spectra of MCM-41@Fe<sub>3</sub>O<sub>4</sub>, Dafo-MCM-41@Fe<sub>3</sub>O<sub>4</sub>, and B<sub>12</sub>-Dafo-MCM-41@Fe<sub>3</sub>O<sub>4</sub>.

1680 cm<sup>-1</sup>:1508 cm<sup>-1</sup> is almost two times higher than in the Dafo-MCM-41@Fe<sub>3</sub>O<sub>4</sub>. The characteristic peak of B<sub>12</sub> has strengthened the absorbance in this position suggesting that the drug has been successfully loaded into MCM-41 tunnels.

Thermogravimetric degradation (TGA) is then applied to confirm drug loading in B<sub>12</sub>-Dafo-MCM-41@Fe<sub>3</sub>O<sub>4</sub>, as shown in Figure 9. For comparison purposes, Dafo-MCM-41@Fe<sub>3</sub>O<sub>4</sub> was first test for TGA, there are two major weight loss regions on its TGA curve. Started from 250 °C the organic ligand begins to decompose therefore we got the first weight lost. Then at around 480° the framework left in Dafo-MCM-41@Fe<sub>3</sub>O<sub>4</sub> starts to degrade which results in the second weight lost. In the case of B<sub>12</sub>-Dafo-MCM-41@Fe<sub>3</sub>O<sub>4</sub>, since it is drug loaded. It takes longer to lost weight before the curve reaches the stable stage at around 550°. In the final stage, B<sub>12</sub>-MCM-41@Fe<sub>3</sub>O<sub>4</sub> lost 16% more weight than Dafo-MCM-41@Fe<sub>3</sub>O<sub>4</sub>, which is close to 0.12 mmol/g.

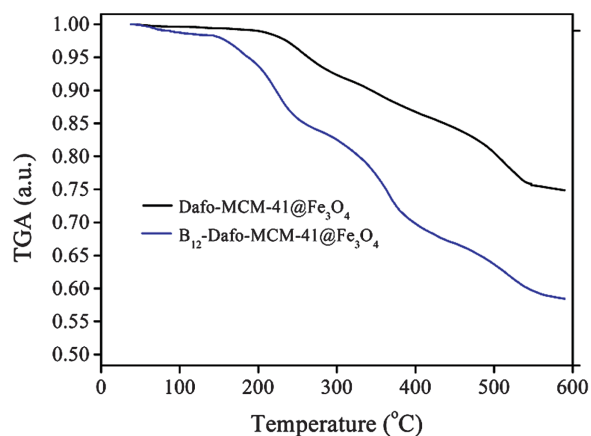


**Figure 9.** TGA of Dafo-MCM-41@Fe<sub>3</sub>O<sub>4</sub> and B<sub>12</sub>-Dafo-MCM-41@Fe<sub>3</sub>O<sub>4</sub>.

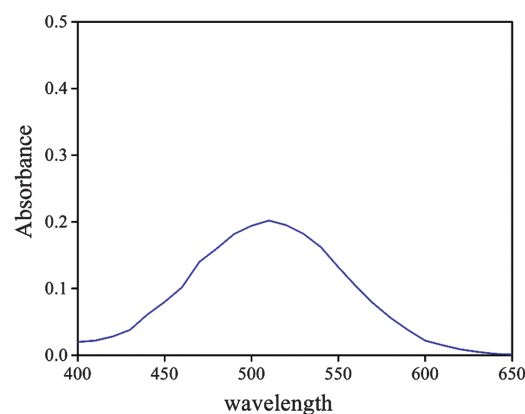


**Figure 10.** Absorbance in visible spectrum of Dafo (2 mmol/mL in ethanol).

### 3.7. Determination of Wavelength

The light controlled release property of the Dafo-MCM-41@Fe<sub>3</sub>O<sub>4</sub> is caused by the flipping of C=N bond, therefore the wavelength of exciting light should be determined. According to the literature,<sup>19</sup> N=N bond has a maximum absorbance at 450 nm in visible spectrum, so we tested the absorbance of Dafo at the range from 400 to 650 nm. As shown in the Figure 10, there is a broad peak in 510 nm and can be assigned to  $\pi$ - $\pi^*$  absorption of C=N bond. As a result, in our experiment, 510 nm LED laser was used as stimulating light to load and release drug molecules.

### 3.8. Drug Release

Figure 11 displays the release behavior of vitamin B<sub>12</sub> from the magnetic drug nanoparticle carrier in simulated body fluids within 60 h. Without light stimulated, drug release starts from 4% in the first half hour and bursts to 11% in 5 hours then slowly increases to 25% in 60 hours. With 510 nm light present, the drug release speed becomes significantly higher. Starts from 10% release rate in the first half hour and bursts to 38% in 10 hours then reaches 59% in the final, which is two and a half times higher than when light off. Therefore, the Dafo-MCM-41@Fe<sub>3</sub>O<sub>4</sub> shows light controlled release property. Our nanoparticles

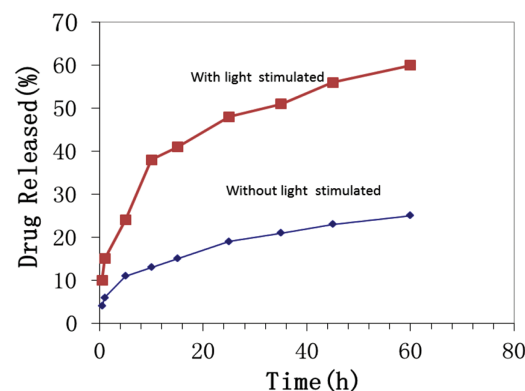


**Figure 11.** Cumulative release of B<sub>12</sub> from Dafo-MCM-41@Fe<sub>3</sub>O<sub>4</sub> with light on and light off.

can release drug molecules on target tissue under light stimulating.

#### 4. CONCLUSION

In conclusion, a core–shell structured composite was modified by an organic ligand with a Dafo end, aiming at releasing drug molecules under light stimulated. Its  $\text{Fe}_3\text{O}_4$  core is responsible for site-specific guiding, its MCM-41 shell serves as supporting matrix for drug carrier. This structure was analyzed and confirmed by SEM, TEM, XRD, IR spectra, TGA and  $\text{N}_2$  adsorption/desorption. Drug carrier's cytotoxicity was studied by MTT using L929 fibroblast cell, and low cytotoxicity was revealed. Magnetic measurements show that these composites exhibit sufficient reactivity under external magnetic field. The Dafo-MCM-41@ $\text{Fe}_3\text{O}_4$  composite shows light controlled release behaviors for vitamin  $\text{B}_{12}$  *in vitro*. It has 2.5 times faster release rate when light present than without light stimulated. We tentatively concluded that Dafo-MCM-41@ $\text{Fe}_3\text{O}_4$  can be potential vectors for drug delivery.

**Acknowledgment:** The authors gratefully thank our universities for their equipments and financial support.

#### References and Notes

1. M. Malaguarnera, R. Ferri, R. Bella, G. Alagona, A. Carnemolla, and G. Pennisi, *Clin. Chem. Lab. Med.* **42**, 1032 (2004).
2. L. Meertens, N. Diaz, L. Solano, M. Barón, and A. Rodríguez, *Arch. Latinoam. Nutr.* **57**, 26 (2007).
3. Q. He and J. Shi, *J. Mater. Chem.* **21**, 5845 (2011).
4. Y. Hu, Z. Wang, T. Zhi, and S. Jiang, *J. Colloid Interface Sci.* **363**, 410 (2011).
5. E. Niemea, D. Desaib, Y. Nkizinkikoa, J. E. Erikssona, and J. M. Rosenholmb, *European J. Pharm. Biopharm.* **96**, 11 (2015).
6. N. Hao, F. Tang, and L. Li, *Microporous and Mesoporous Materials* **218**, 25 (2015).
7. X. Chen, X. Yao, C. Wang, L. Chen, and X. Chen, *Microporous and Mesoporous Materials* **217**, 46 (2015).
8. A. Tamayo, M. Mazo, A. Ruiz-Caro, R. Martín-Illana, A. Bedoya, and L. M. Veiga-Ochoa, *Chem. Engineering J.* **280**, 165 (2015).
9. Y. Cai, L. Ling, X. Li, M. Chen, and L. Su, *J. Solid State Chem.* **226**, 179 (2015).
10. S. Huang, C. Li, Z. Cheng, Y. Fan, P. Yang, C. Zhang, K. Yang, and J. Lin, *J. Colloid and Interface Science* **376**, 312 (2012).
11. Y. Ma, Y. Gao, Y. Wang, Y. Li, and X. Yang, *Modern Applied Science* **5**, 232 (2011).
12. Y. Wang, B. Li, L. Zhang, P. Li, L. Wang, and J. Zhang, *Langmuir* **28**, 1657 (2012).
13. Y. Deng, D. Qi, C. Deng, and X. Zhang, *J.A.C.S* **130**, 28 (2008).
14. L. Zhang, W. Sun, and P. Cheng, *Molecules* **8**, 207 (2003).
15. K. Michal and M. Jaroniec, *Chemistry of Materials* **13**, 3169 (2001).
16. K. Michal, M. Jaroniec, and A. Sayari, *Chemistry of Materials* **11**, 492 (1999).
17. S. Huang, C. Li, Z. Cheng, Y. Fan, P. Yang, C. Zhang, K. Yang, and J. Lin, *J. Colloid and Interface Science* **376**, 312 (2012).
18. Y. Cai, L. Ling, X. Li, M. Chen, and L. Su, *J. Solid State Chem.* **226**, 179 (2015).
19. L. Zhang, S. Yue, B. Li, and D. Fan, *Inorg. Chim. Acta.* **384**, 225 (2012).

Received: 7 August 2015. Accepted: 18 January 2016.